Supplementary: Temperature dependent study of the spin dynamics of coupled $Y_3Fe_5O_{12}/Gd_3Fe_5O_{12}/Pt$ trilayers

Felix Fuhrmann, Sven Becker, Akashdeep Akashdeep, and Gerhard Jakob

Institute of Physics, University of Mainz,

Staudingerweg 7, Mainz 55128, Germany

Qianqian Lan, Nan Wang, and Rafal E. Dunin-Borkowski

Ernst Ruska-Centre for Microscopy and Spectroscopy with Electrons (ER-C-1),

Forschungszentrum Jülich GmbH, 52425 Jülich, Germany

Romain Lebrun

Unité Mixte de Physique, CNRS, Thales,

Université Paris-Saclay, F-91767 Palaiseau, France

Mathias Weiler

Fachbereich Physik and Landesforschungszentrum OPTIMAS,

Rheinland-Pfälzische Technische Universität

Kaiserslautern-Landau, 67663 Kaiserslautern, Germany

Mathias Kläui

Institute of Physics, University of Mainz,

Staudingerweg 7, Mainz 55128, Germany

Graduate School of Excellence "Materials Science in Mainz" (MAINZ),

Staudingerweg 9, Mainz 55128, Germany and

Center for Quantum Spintronics, Norwegian University

of Science and Technology, Trondheim 7491, Norway

(Dated: July 1, 2025)

TEMPERATURE DEPENDENCE IN SINGLE GDIG LAYERS

Resonance spectra from VNA-FMR measurements for single GdIG layers are shown in supplementary Fig. 1. For single GdIG layers, the signal is only clearly visible for low temperatures (below 100 K)

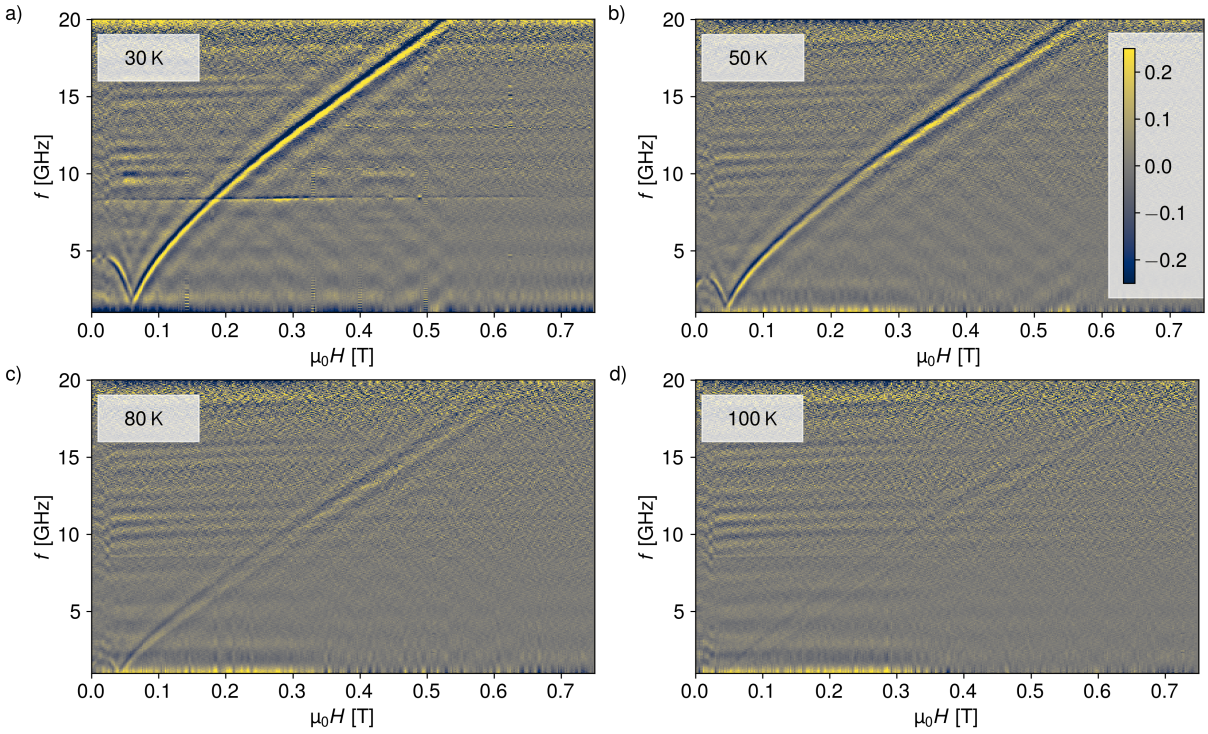

Supplementary Figure 1. The raw data is processed by derivative divide and an FFT-filter. Progessively weaker signals are observed for higher temperatures.

INTERFACE QUALITY

To judge the quality of the heterostructe and the interfaces, we performed high-angle annular dark-field (HAADF) scanning transmission microscopy (STEM) measurements. From these images (supplementary Figure 2) we can extract more information about the crystallinity of the individual layers and the interface. Suppl. Fig. 2 a) shows a HAADF–STEM image of the GdIG (brighter contrast) on YIG (darker contrast) film, demonstrating excellent film quality with no visible defects and a sharp interface. In HAADF–STEM, the detected intensity I scales approximately as $Z^{1.7}$, where Z is the atomic number. From the

image in Suppl. Fig. 2 a), we extracted a line profile across the interface, which is presented in Suppl. Fig. 2 b). The transition region highlighted in yellow indicates the maximum expected range where interdiffusion of atoms occurs.

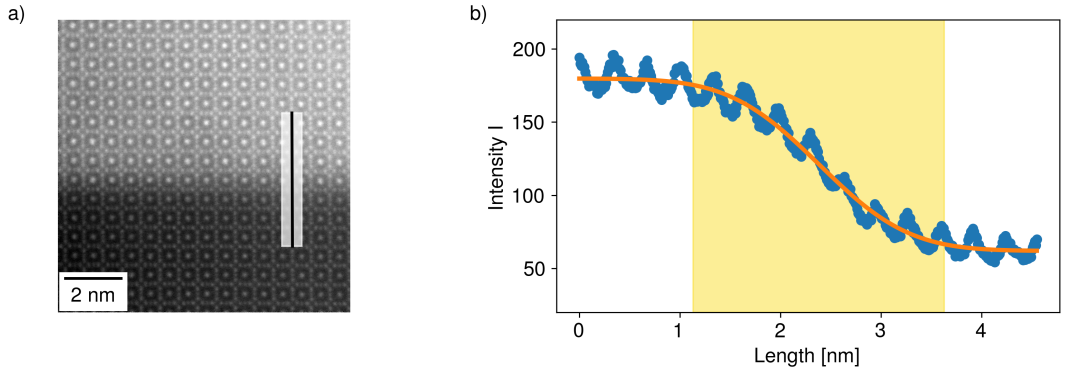

Supplementary Figure 2. a) HAADF-STEM image across the interface between GdIG (top) and YIG (bottom) layer. The measured sample consist of GGG/YIG [17 nm]/GdIG [17 nm] capped with Au. The top half of the STEM image with a lighter contrast shows the extent of the GdIG layer, the lower half with the darker contrast is the YIG layer. b) Extracted line profile as indicated in the STEM image across the YIG/GdIG interface, with the orange line as the fit result of the equation 2. The yellow region marks the extent of two lattice constants.

One can fit an error function $f_{\mathrm{erf}}(x)$ the extracted lineprofile to extract the width of this transition.

$$f_{\mathrm{erf}}(x) = \frac{A}{2}\left[1 + \mathrm{erf}\left(\frac{x-\mu}{\sigma}\right)\right] \tag{1}$$

With μ as the center of the transition, σ as the characteristic width and A as the amplitude. We can estimate the width of the transition by calculating the full width half maximum (FWHM) of the derivative $\frac{df_{\mathrm{erf}}(x)}{dx}$ of the function $f_{\mathrm{erf}}(x)$.

$$\frac{df_{\mathrm{erf}}(x)}{dx} = \frac{A}{\sigma\sqrt{\pi}} \exp\left(-\left(\frac{x-\mu}{\sigma}\right)^2\right) \tag{2}$$

This gives us the dependence of the FWHM on σ.

$$\mathrm{FWHM} = 2\sigma\sqrt{\ln 2} \approx 1.665\sigma \tag{3}$$

For our YIG/GdIG interface, the FWHM is (1.65 ± 0.04) nm.

To put this range in perspective, it is comparable but smaller to the extent of two times the lattice constant of YIG and GIG with $a = 1.2\,\mathrm{nm}$. Thus, the 2.5 nm as marked in the lineprofile (Suppl. Fig. 2 b) are the upper limit of roughness and possible diffusion between the two layers.

DAMPING PARAMETER EXTRACTION FOR SINGLE YIG LAYER

To estimate the damping parameter, we acquired a resonance spectrum from VNA-FMR measurements for a single YIG layer (supplementary Fig. 3 a). The YIG layer has a thickness of 36 nm and is grown by PLD with comparable growth parameters as the heterostructure, discussed in the main text.

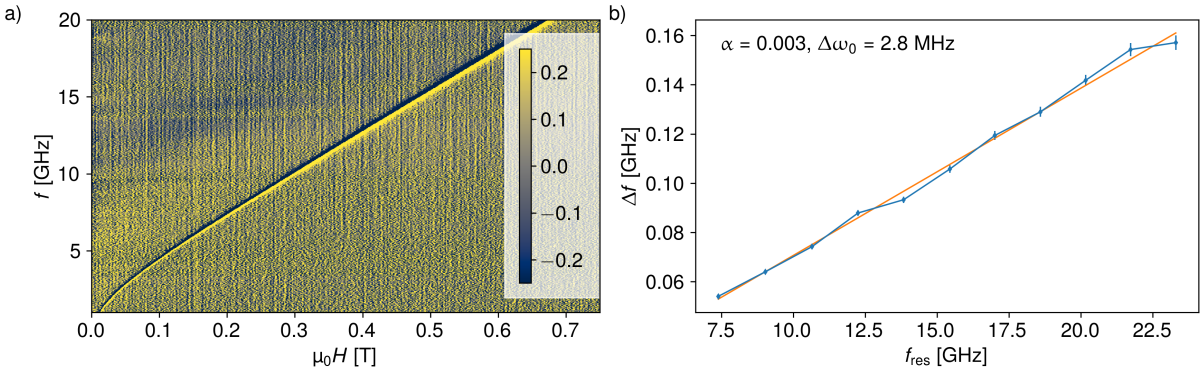

Supplementary Figure 3. a) The raw data from measurement in a room temperature FMR setup is processed by derivative divide for the plotting of the FMR spectrum. b) Extracted linewidth plotted against the resonance frequency f_{res} with fitted Gilbert damping parameter α for the same measurement.

The linewidth is extracted with the derivative of the formula of the susceptibility χ [4].

$$\frac{d\chi}{df} = fAe^{i\psi}\frac{2f + i\Delta f_{\mathrm{FWHM}}}{\left(-f^2 - if\Delta f_{\mathrm{FWHM}} + f_{\mathrm{res}}^2\right)^2} + \frac{Ae^{i\psi}}{-f^2 - if\Delta f_{\mathrm{FWHM}} + f_{\mathrm{res}}^2} + \mathrm{const.} \tag{4}$$

With the resonance frequency f_{res}, the full width half maximum Δf_{FWHM}, phase angle ψ of the signal and amplitude A.

A Gilbert-like model is then used to extract the damping of our film [5, 6].

$$\Delta\omega = 2\alpha\omega + \Delta\omega_0 \tag{5}$$

With this formula, we can evaluate the linewidth $\Delta\omega$, extract the damping parameter α and inhomogeneous broadening $\Delta\omega_0$.

The extracted linewidth is plotted in supplementary Fig. 3 b), the extracted damping parameter was later used for the simulation and is comparable to other PLD grown YIG samples [7]

NUMERICAL SIMULATION: MACRO-SPIN MODEL

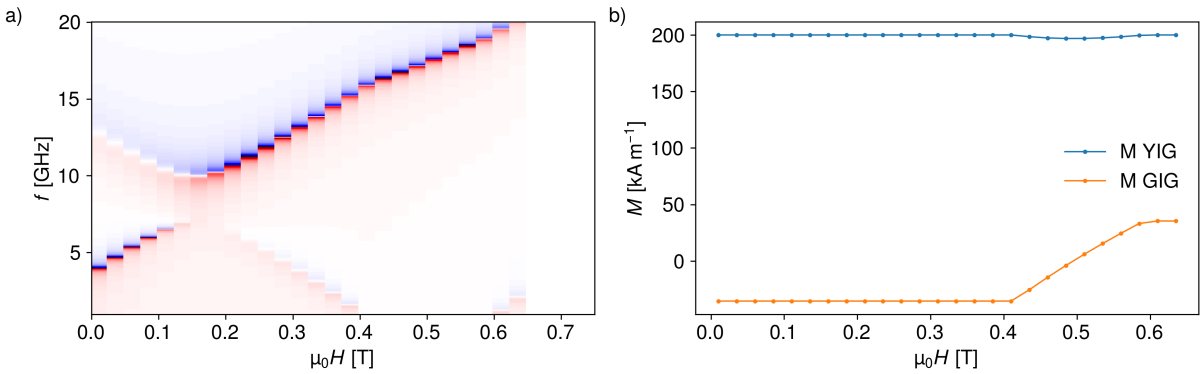

Supplementary Figure 4. a) Dynamic response spectrum for macrospin model with two spins, with M_s estimated for 220 K b) Static reorientation behavior for the GdIG layer magnetization during the macrospin model simulation.

In order to understand the experimental result, we follow the model from Ref. [1] and use the 1-2-3 coordinate system [2]. In this coordinate system, the equilibrium direction of the magnetization defines the 3-direction, with the dynamic components along the 1- and 2-axes. We consider 2 macro spins in the model. One for the combined sublattices of YIG S_{YIG} and one for the combined sublattices of GdIG S_{GdiG}. We extend the model with the dipolar interaction between S_{YIG} and S_{GdiG}. We assume damping parameters for similarly grown single layers of YIG and GdIG via PLD. The numerical model is set up in Mathematica as an eigenvalue problem of the 4×4 susceptibility matrix $\overleftrightarrow{\chi}$, with the components of the oscillating driving field $h^{1,2,3}$ and the magnetization $m'^{1,2,3}$ for each sublattice.

$$h^{1,2,3} = \overleftrightarrow{\chi}^{-1} m'^{1,2,3} \tag{6}$$

We solve the susceptibility matrix for a range of external magnetic fields and resonance

frequencies to create a colormap-image, similar to the experimental FMR data. The equilibrium state of the macro-spins is obtained by minimizing the free energy F.

$$\begin{aligned} F = &- \mu_0 \lambda_{YG} \mathbf{M}_{Y,xyz} \cdot \mathbf{M}_{G,xyz} \\ &- \mu_0 \mathbf{H}_0 \cdot \mathbf{M}_{T,xyz} \\ &+ \frac{\mu_0}{2} \mathbf{N}_{demag} \cdot \mathbf{M}_{T,xyz} \cdot \mathbf{M}_{T,xyz} \end{aligned} \tag{7}$$

With the coupling constant λ_{YG} for the coupling between $\mathbf{M}_{Y_{xyz}}$ and $\mathbf{M}_{G_{xyz}}$, the magnetization of YIG $\mathbf{M}_{Y_{xyz}}$, GdIG $\mathbf{M}_{G_{xyz}}$ and the total magnetization $\mathbf{M}_{T_{xyz}} = \mathbf{M}_{Y_{xyz}} + \mathbf{M}_{G_{xyz}}$, the demagnetization tensor $\mathbf{N}_{demag}$ and the magnetic permeability μ_0.

The following formulas are written for the YIG (Y) macro-spin, but are analogous for the GdIG (G) macro-spin. The free energy for the macro-spins in the respective equilibrium (123) coordinate system is written in the following form.

$$\begin{aligned} F_Y = &- \mu_0 \lambda_{YG} \mathbf{M}_{Y,Y123} \cdot \mathbf{M}_{G,Y123} \\ &- (\mathbf{U}_Y^{-1} \cdot \mu_0 \mathbf{H}_0) \cdot \mathbf{M}_{T,Y123} \\ &+ \frac{\mu_0}{2} (\mathbf{z}_{Y123} \cdot \mathbf{M}_{T,Y123})^2 \end{aligned} \tag{8}$$

$\mathbf{M}_{G,Y123}$ is $\mathbf{M}_G$ in the 123-coordinate system of the YIG (Y) equilibrium position. The transformation matrix $\mathbf{U}_Y^{-1}$ translates the external applied magnetic field into the YIG 123-coordinate system. The resulting demagnetization term by $\mathbf{N}_{demag}$, is parallel to the thin film orthogonal $\mathbf{z}_{Y123}$.

The free energy for the respective layer is then used to calculate an effective field $\mathbf{H}_{eff,Y}$, including the alternating driving field $\mathbf{h}_Y$.

$$\begin{aligned} \mu_0 \mathbf{H}_{eff,Y} = &- \left\{ \frac{\partial F_Y}{\partial m_{Y1}(t)}, \frac{\partial F_Y}{\partial m_{Y2}(t)}, \frac{\partial F_Y}{\partial m_{Y3}} \right\} \\ &+ \mu_0 \left\{ h_{Y1} e^{i\omega t}, h_{Y2} e^{i\omega t}, 0 \right\} \end{aligned} \tag{9}$$

$\mathbf{H}_{eff,Y}$ is then included as the effective field in the Landau Lifshitz Gilbert (LLG) equation for the respective layer. The phenomenological damping constant α_Y is introduced for each layer.

$$\frac{d}{dt}\mathbf{m}_{Y,123} = -\gamma_Y \mathbf{m}_{Y,123} \times \mu_0 \mathbf{H}_{eff,Y} + \alpha_Y \mathbf{m}_{Y,123} \times \frac{d\mathbf{m}_{Y,123}}{dt} \tag{10}$$

In these simulations, the values for magnetization of the YIG and GdIG film are extracted from literature [3]. The results (supplementary Figure 4) are also in reasonable agreement with the experimental data.

MICROMAGNETIC SIMULATION

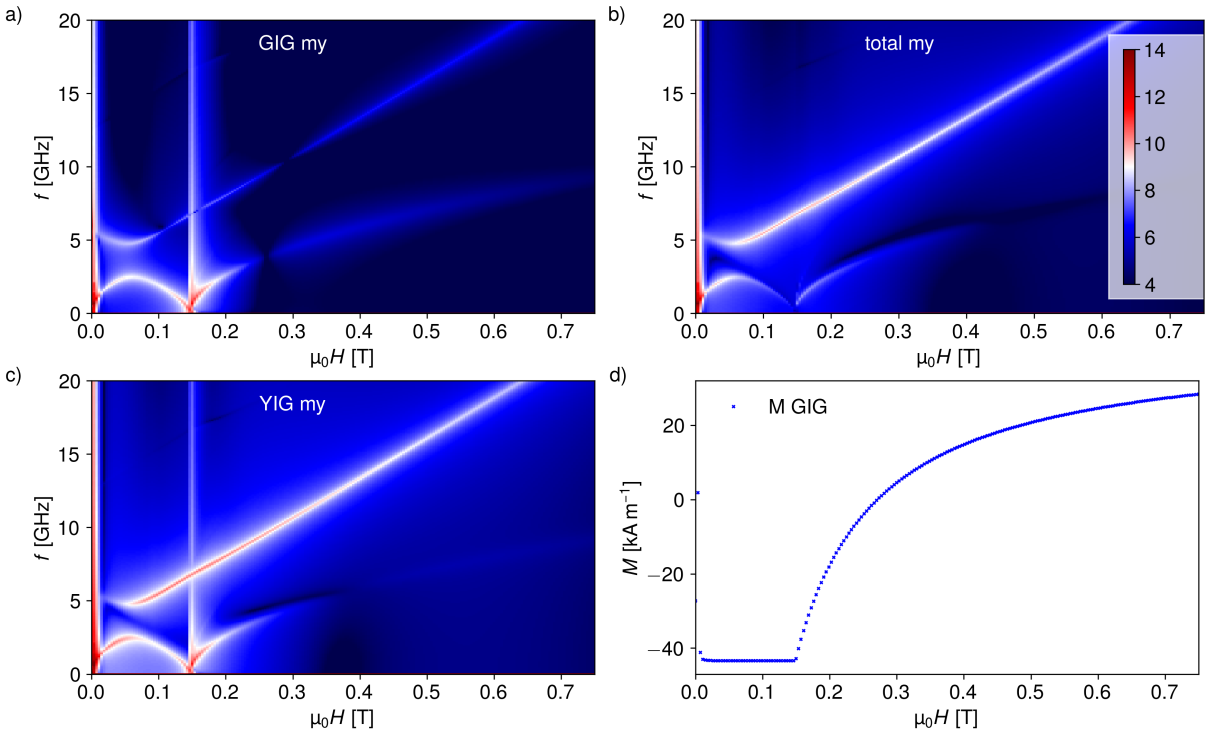

Supplementary Figure 5. Dynamic spectrum from micromagnetic simulations for the value of M_s for 220 K the y component of a) YIG, b) GdIG and c) the total magnetization. The static magnetization from the simulation for the switching layer GdIG is plotted in d).

The micromagnetic simulations are performed with the ubermag package [8]. In this package, one can easily switch between OOMMF and Mumax3 [9]. Both solvers return compatible spectra, however because of the more time efficient simulations of mumax3, we

used mainly mumax3 for the simulations in this paper. The cellsize of the mesh is chosen to be smaller than the exchange length $\lambda_{ex} = \sqrt{\frac{2A}{\mu_0 M_s^2}}$ of YIG ($\approx$13 nm for the x and y directions [10]. With A as the exchange constant of YIG and M_s, the saturation magnetization. For the z-direction one can expect a more complicated spin-structure, thus the cellsize was further reduced, to capture also non-trivial spin structures. Thus, the cellsize was chosen to be 10 nm x 10 nm x 3 nm. The system was designed to be 0.15 µm laterally in x and y direction with periodic boundary conditions in x and y direction, and the two film thicknesses were set to 36 nm for YIG and 30 nm for GdIG. The exchange coupling for YIG is set to 3.17 pJ m^{-1}, while the exchange coupling for GdIG is set to a reduced value of 2.5 pJ m^{-1}. The exchange coupling between YIG and GdIG is set phenomenologically to -1.2 pJ m^{-1}.

The micromagnetic simulation allows us to extract the spectrum for each component of each layer. The z and y components are the most relevant for us, as our sample is placed on a coplanar waveguide in the experiment. The alternating magnetic field components are mainly in y-direction, with a small out of plane component (z-direction). The static magnetic field is applied in x-direction (for the reference system in the simulation). Thus, this component is the least relevant for us. For spin pumping measurements, the relevant component is in y-direction. This is also well compatible with our assumption from the main text, that during the reorientation of the GdIG magnetization, we do not observe any spin-pumping signal. This is in line with the feature in supplementary Figure 5 b), in which we can see the reduction of the amplitude of the mode during the magnetization reorientation of the GdIG layer supplementary Figure 5 d).

We can clearly see, that the reorientation of the GdIG magnetization obtained from the micromagnetic simulation (supplementary Fig. 4) closely matches the experimental observation, while that from the macrospin model (supplementary Fig. 1b) is only in qualitative agreement (supplementary Fig. 6).

The micromagnetic simulation suggests a helical spin structure in the GdIG layer during and after the switching (supplementary Figure 7), which is in agreement with the conclusion in Reference [11].

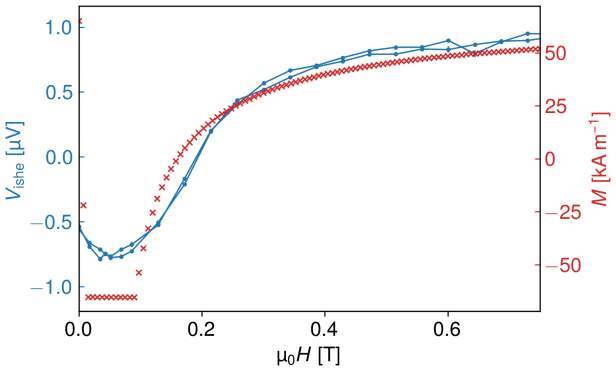

Supplementary Figure 6. Spin Seebeck effect measurement (blue), to extract the magnetization reorientation behavior of GdIG, at 180 K, compared to the extracted magnetization of GdIG from the micromagnetic stimulation. The magnetization is estimated from literature to match a temperature of 195 K (red), the offset of 15 K is chosen to account for the shifted compensation temperature when comparing the literature values of bulk crystals and our thin films.

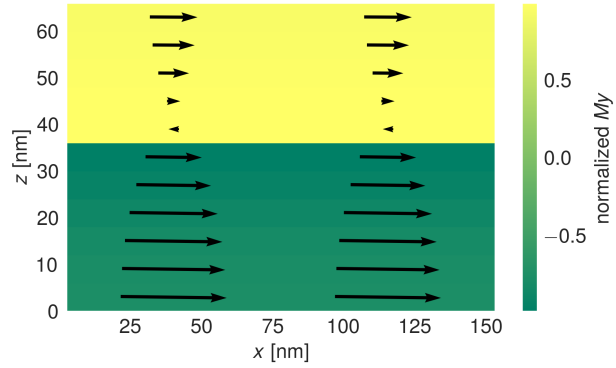

Supplementary Figure 7. Cut through the x-z-plane of the mesh of the micromagnetic simulation at 120 K, revealing a helical state in the top (GdIG) layer, with a sufficiently large applied magnetic field of 0.18 T. The number of arrows is reduced compared to the number of cells in the simulation for clarity.

BIBLIOGRAPHY

[1] L. Liensberger, A. Kamra, H. Maier-Flaig, S. Geprägs, A. Erb, S. T. Goennenwein, R. Gross, W. Belzig, H. Huebl, and M. Weiler, Phys. Rev. Lett. **123**, 117204 (2019).

[2] L. Dreher, M. Weiler, M. Pernpeintner, H. Huebl, R. Gross, M. S. Brandt, and S. T. B. Goennenwein, Phys. Rev. B **86**, 134415 (2012).

[3] G. F. Dionne, *Magnetic oxides* (Springer, New York, NY, 2009).

[4] M. L. Schneider, J. M. Shaw, A. B. Kos, T. Gerrits, T. J. Silva, and R. D. McMichael, Journal of Applied Physics **102**, 103909 (2007).

[5] H. Maier-Flaig, S. T. B. Goennenwein, R. Ohshima, M. Shiraishi, R. Gross, H. Huebl, and M. Weiler, Rev. Sci. Instrum. **89**, 076101 (2018).

[6] T. D. Rossing, Journal of Applied Physics **34**, 995 (1963).

[7] R. Kumar, B. Samantaray, S. Das, K. Lal, D. Samal, and Z. Hossain, Phys. Rev. B **106**, 054405 (2022).

[8] M. Beg, M. Lang, and H. Fangohr, IEEE Transactions on Magnetics **58**, 1 (2022).

[9] A. Vansteenkiste, J. Leliaert, M. Dvornik, M. Helsen, F. Garcia-Sanchez, and B. Van Waeyenberge, AIP Advances **4**, 107133 (2014).

[10] G. Venkat, H. Fangohr, and A. Prabhakar, Journal of Magnetism and Magnetic Materials **450**, 34 (2018), perspectives on magnon spintronics.

[11] J. M. Gomez-Perez, S. Vélez, L. McKenzie-Sell, M. Amado, J. Herrero-Martín, J. López-López, S. Blanco-Canosa, L. E. Hueso, A. Chuvilin, J. W. A. Robinson, and F. Casanova, Phys. Rev. Applied **10**, 044046 (2018).